Photocatalysis

DOI: 10.1002/anie.201302329

Nanoporous Nitrogen-Doped Titanium Dioxide with Excellent Photocatalytic Activity under Visible Light Irradiation Produced by Molecular Layer Deposition**

Chaoqiu Chen, Ping Li, Guizhen Wang, Yu Yu, Feifei Duan, Caiying Chen, Weiguo Song, Yong Qin, and Mato Knez**

Molecular layer deposition (MLD) is a processing technology for depositing ultrathin polymer or inorganic–organic hybrid films. It is a subset of atomic layer deposition (ALD) and has attracted tremendous attention because of its self-limiting nature, excellent conformality, chemical selectivity and low reaction temperature.[1–6] However, because of factors like low vapor pressure and thermal sensitivity of many organic molecules and poor understanding of vapor-phase organic coupling reactions,[7] the variety of combinations of organic and inorganic reactants that have been used for successful MLD is sparse. Up to now, only a few organic–inorganic polymer films, including alucone,[8–11] zincone,[12] and titanicone,[13,14] have been grown through MLD and those were mainly based on reactions between metal alkyl/chloride and glycol/glycerol. Given the great promise of MLD, it is highly demanded to develop new processing strategies for MLD.

One important aspect for producing a larger range of organic–inorganic mixtures is the variability of compositions of the constituting organic and inorganic fractions of the resulting films. A limitation to rather short organic spacers, such as glycol, between the metal ions is a bottleneck for the synthesis of films with a broader range of organic–inorganic volume ratios. By designing new processing strategies for the organic component, the properties of the resulting films can be more easily tuned by varying their composition. These organic–inorganic hybrid films can be further used to produce porous metal oxide films by removing the organic component and the porosity of the resulting inorganic films will depend on the volume occupied by the organic constituting part, making such films attractive for many applications such as catalysis, separation, sensing, and energy conversion and storage.

As an important semiconductor, TiO_2 has been intensely investigated using various ALD processes for its evident application potential in solar-energy devices, environmental remediation, and as catalyst support.[15–20] However, due to the ALD growth characteristics these TiO_2 films are intrinsically pinhole-free with low specific surface areas, resulting in low photocatalytic activity.[19,20] Recently, the research groups of George, Yerushalmi, and our group reported nearly in parallel the successful preparation of porous TiO_2 by annealing or UV exposure of Ti-containing hybrid organic–inorganic films (titanicones) produced by MLD using $TiCl_4$ and glycol or glycerol as reactants.[13,14,21] However, their activity is only efficient with ultraviolet light irradiation because of the wide band gap of TiO_2 (3.2 eV for anatase). Therefore, developing new MLD processes to grow porous TiO_2 films with visible light response and larger surface area is very welcome for such applications.

Herein, we demonstrate a novel MLD process for preparing porous N-doped TiO_2 films. The process is based on a new strategy, a four-step ABCB reaction sequence using titanium tetrachloride ($TiCl_4$, precursor A), ethanolamine (EA, precursor B), and malonyl chloride (MC, precursor C) as the reactants. The reaction includes a hetero-bifunctional and a homo-bifunctional organic precursor, both ensuring certain selectivity of coupling reactions in each step of the process. Furthermore, this synthesis strategy is also successfully applied to the growth of nanoporous Al_2O_3 films by replacing $TiCl_4$ with trimethylaluminum (TMA) as a metal-containing precursor. The shown strategy allows a combinatorial approach to organic–inorganic hybrid materials through control of the coupling by controlling the surface functional groups. In this way it becomes possible to still maintain the self-limited growth conditions. The four coupling sites used in this work (metal halide, acyl chloride, amine, and alcohol) offer a wide variety of tuning possibilities for the composition of the organic–inorganic hybrid film. In addition,

[*] Dr. C. Q. Chen, G. Z. Wang, F. F. Duan, C. Y. Chen, Prof. Y. Qin
State Key Laboratory of Coal Conversion
Institute of Coal Chemistry
Chinese Academy of Sciences, Taiyuan 030001 (P.R. China)
E-mail: qinyong@sxicc.ac.cn
P. Li, Y. Yu, Prof. W. G. Song
Beijing National Laboratory for Molecular Sciences (BNLMS)
Institute of Chemistry, Chinese Academy of Sciences
Beijing, 100190 (P.R. China)
Prof. M. Knez
CIC nanoGUNE Consolider, Tolosa Hiribidea 76
20018 Donostia-San Sebastian (Spain) and
IKERBASQUE, Basque Foundation for Science
Alameda Urquijo 36-5, 48011 Bilbao (Spain)
E-mail: m.knez@nanogune.eu

[**] This work was financially supported by the Natural Science Foundation of Shanxi Province, China (grant number 2013011012-6), National Natural Science Foundation of China (grant number 21173248 and 21203229), the Hundred Talent Program of the Chinese Academy of Sciences, and an in-house project of the State Key Laboratory of Coal Conversion of China (grant numbers Y1BWLI1991 and Y2BWLD1931). We thank Ms. Yunmei Li, Dr. Junfeng Zhang, and Prof. Jianli Yang for Fourier transform infrared characterization and analysis.

Supporting information for this article is available on the WWW under http://dx.doi.org/10.1002/anie.201302329.

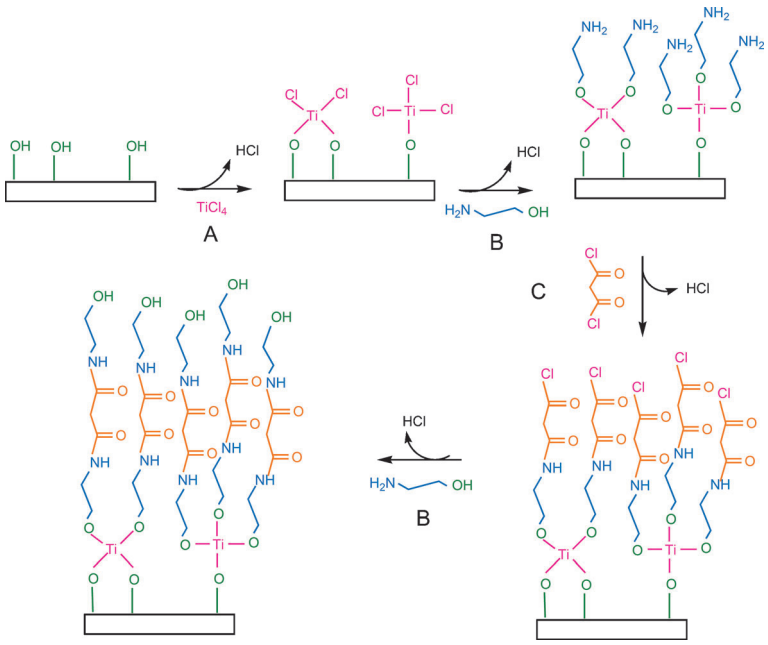

Figure 1. Four-step ABCB reaction sequence for Ti-hybrid film formation using $TiCl_4$, EA, and MC as molecular precursors.

the amine group introduced in this process allows in situ doping of the TiO_2 with nitrogen.

Figure 1 shows a proposed reaction sequence during this four-step ABCB MLD process for the Ti-hybrid film growth. Firstly, $TiCl_4$ reacts with hydroxy groups on the substrate surface to form -$TiCl_x$ species. Secondly, the hydroxy end of the EA reacts preferentially with the -$TiCl_x$ species resulting in a -$OCH_2CH_2NH_2$ terminated surface, which subsequently anchors the MC in the following third step to form a new surface species terminated by acyl chloride. In the final step, the amino end of the EA reacts preferentially with the surface-terminating acyl chloride groups to reform hydroxy groups on the surface, closing one deposition cycle. The four-step ABCB sequence is repeated in a desired number to grow the hybrid films. After annealing in a H_2/Ar atmosphere, N-doped TiO_2 nanoporous films were obtained from the films described above. The process enables tuning of the distance between adjacent Ti moieties through the length of the organic linkers.

Herein, suspended CuO nanowires, grown on transmission electron microscope (TEM) Cu grids (3.05 mm in diameter, Plano, Germany) by heating in air,[22] were used as substrates for the deposition of hybrid films and were for convenience directly applied for subsequent TEM analysis. Figure 2a shows a TEM image of the produced Ti-hybrid/CuO nanowires. The Ti-hybrid film grown with a thickness of about 30 nm after 50 MLD cycles is very smooth, uniform, and conformal, as expected from the self-limiting growth of the molecular layers.[23] After annealing in H_2/Ar at 600 °C for 2 h, porous TiO_2 nanotubes are obtained, as shown in Figure 2b and 2c. The substrate CuO nanowires disappear and Cu particles are observed at the terminal ends of the porous TiO_2 nanotubes as a result of out-diffusion (see detailed information in Figure S1 in the Supporting Information). The selected-area electron diffraction pattern (SAED, inset in Figure 2b) and the high-resolution TEM image (Figure 2d) reveal the polycrystalline nature of these TiO_2 nanotubes. The observed diffraction rings agree well with the lattice spacing of the TiO_2 crystals.

To investigate the photocatalytic activity of the nanoporous TiO_2 film, carbon nanocoils (CNCs) were selected as substrates for Ti-hybrid film deposition because of their high surface area and good electrical conductivity. Uniform coatings of the CNCs are easily obtained because of the abundant surface defect sites,[24,25] which are in contrast to the inert surface of pristine carbon nanotubes.[26] Figure 2e shows the morphology of uncoated CNCs with diameters of about 100 nm, having a uniform contrast. After applying 50 ABCB cycles of MLD, a conformal and uniform film with a thickness of about 30 nm is successfully deposited onto the surface of the CNCs, clearly visible from the darker contrast as compared to the pristine CNCs (Figure 2f). The film deposited after 50 MLD cycles was analyzed using Fourier transform infrared spectroscopy (FT-IR). The

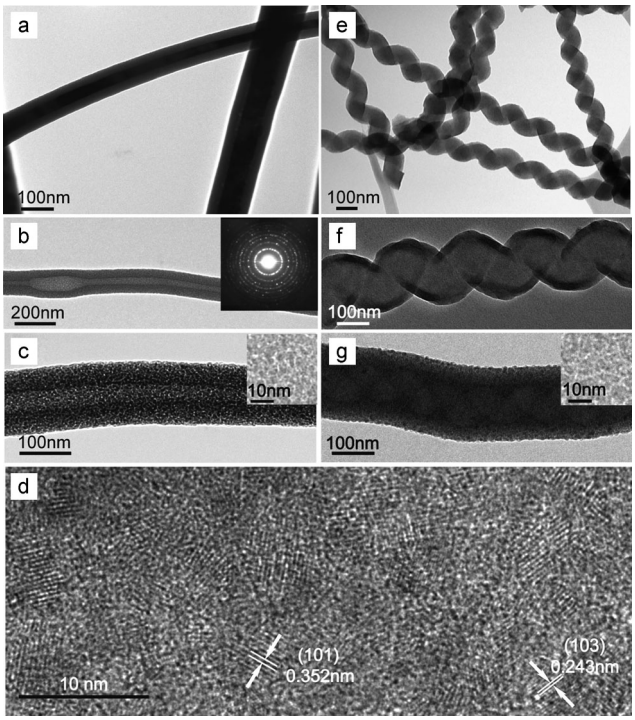

Figure 2. a) TEM image of Ti-hybrid/CuO nanowires obtained after 50 ABCB MLD cycles. b) Low-magnification TEM image of nanoporous N-doped TiO_2 nanotubes obtained after 100 ABCB MLD cycles on CuO nanowires following annealing at 600 °C in H_2/Ar (inset: corresponding SAED pattern). c) High-magnification TEM image of nanoporous N-doped TiO_2 nanotubes. d) HRTEM image of N-doped TiO_2 nanotubes. e) TEM image of CNCs. f) TEM image of Ti-hybrid/CNCs obtained after 50 ABCB MLD cycles. g) Low-magnification TEM image of nanoporous N-doped TiO_2/CNCs obtained after 100 ABCB MLD cycles following annealing at 600 °C in H_2/Ar (inset: corresponding high-magnification TEM image).

observed FT-IR absorbance peaks (Figure S2 in the Supporting Information) confirm the successful covalent bonding of EA and MC and the formation of the new Ti-hybrid film using the four-step ABCB reaction sequence.

Similar to above, the Ti-hybrid MLD films on the surface of CNCs were transformed to porous inorganic oxide films by annealing in a H_2/Ar atmosphere (Figure 2g). The porous structure is not clearly seen with TEM at low magnification because of the interference of the CNCs and carbon-coated Cu grids which support the TiO_2/CNCs during TEM analysis. However, the high-magnification TEM image confirms that the TiO_2 shell is porous (inset in Figure 2g). It should be noted that the outer surfaces of the TiO_2/CNCs obtained after applying 100 MLD cycles are not coiled any more. This is resulting from the conformal growth on curved substrates, which can blunt or smoothen sharp asperities and surface features with an increasing film thickness.[27] In contrast to annealing in H_2/Ar, annealing of the Ti-hybrid MLD film/CNCs in air at 600 °C failed to produce porous nanotubes (see Figure S3 in the Supporting Information). This is because of the aggregation of TiO_2 nanoparticles through Ostwald ripening at high temperatures, resulting in the collapse of the TiO_2 nanotubes and pore structures. Upon annealing in a H_2/Ar atmosphere, the porous structure of the TiO_2 films is maintained even at high temperatures. It is possibly because of the generation of amorphous carbon on the TiO_2 surface by decomposition of the organic component, which can prevent the aggregation of TiO_2 at high temperatures. This novel ABCB MLD method is also compatible with further metal-containing precursors as shown on the example of nanoporous Al_2O_3 helical nanotubes produced by replacing $TiCl_4$ with trimethylaluminum with otherwise identical procedure (see Figure S4 in the Supporting Information).

X-ray photoelectron spectroscopy (XPS) measurements were performed to determine the composition of the Ti-hybrid/CNC composites and the resulting porous N-doped TiO_2/CNCs. Figure 3a shows the presence of titanium, oxygen, nitrogen, and carbon atoms in the XPS survey spectra for the Ti-hybrid/CNCs, which is consistent with the above-mentioned FT-IR results. In addition, a weak peak at about 198.16 eV is observed, indicating the presence of chlorine impurities, which was also observed by George and co-workers in their previous reports for titanicone films grown using $TiCl_4$ and EG.[13] The N 1s peak in the XPS spectra of the Ti-hybrid/CNCs is fitted into two peaks centered at 399.46 and 401.48 eV (Figure 3b), corresponding to amide[28] and protonated amine.[29] According to Figure 1, the MLD process should only contain amide incorporated into the Ti-hybrid film. The protonated amines may result from a reaction between amine and HCl, considering the fact that the HCl is the main by-product during the MLD deposition.[4] After annealing at 600 °C in a H_2/Ar atmosphere and removal of the organic part of the film, the nitrogen signal is observed at 399.53 eV (Figure 3b), which can be ascribed to nitrogen most likely located in an interstitial site in TiO_2, suggesting incorporation of N atoms into the resulting TiO_2 porous films.[30–32]

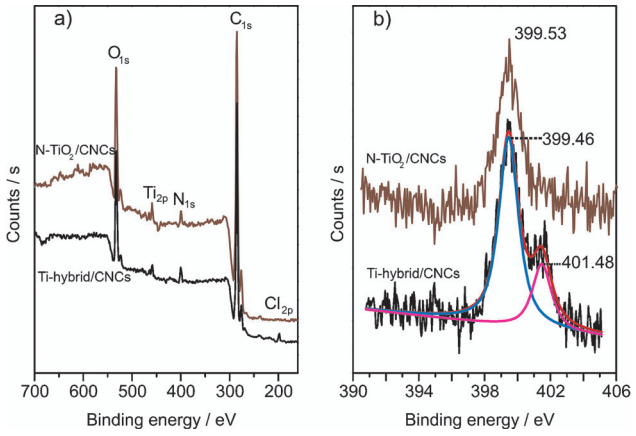

Figure 3. XPS analysis of Ti-hybrid/CNCs and nanoporous N-doped TiO_2/CNCs produced by annealing the Ti-hybrid/CNCs at 600 °C in H_2/Ar. a) XPS survey of the two specimens. b) High-resolution N 1s spectra of the two specimens.

Thermogravimetric analysis coupled with mass spectrometry (TG-MS) in an Ar atmosphere was performed to gain further insight into the decomposition reaction and the products involved during the Ti-hybrid-oxide transformation. The TG and MS profiles for selected gaseous products evolved during heating in argon are shown in Figure 4. The

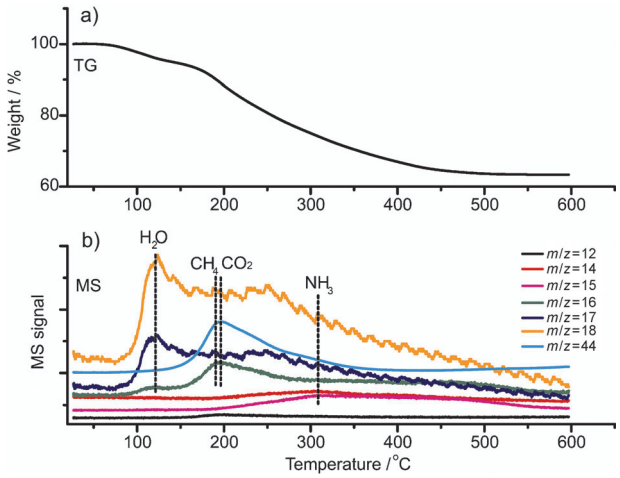

Figure 4. a) TG profiles of Ti-hybrid/CNCs obtained after 200 MLD cycles (heating rate of 10 °C, Ar flux). b) MS profiles of selected gaseous products.

TG plot (Figure 4a) shows two major weight loss regions. The first (up to about 140 °C) can be attributed to desorption of adsorbed water molecules, which is confirmed by MS analysis ($m/z = 18$ and 17, Figure 4b), resulting in a 5 % weight loss. The second weight loss, starting around 160 °C, corresponds to the decomposition of the as-prepared MLD Ti-hybrid film with evolution of CH_4 ($m/z = 16$ and 12), CO_2 ($m/z = 44$), and NH_3 ($m/z = 17$ and 16) which was elsewhere used as nitrogen source for N-doped TiO_2 materials.[33–35] Based on these results, it can be deduced that the substitutional doping of TiO_2 with N atoms occurred through an in situ reaction of TiO_2 with NH_3, which was released during the annealing process.

The photocatalytic activities of the porous N-doped TiO_2/CNCs with varying MLD cycle numbers were evaluated using the photodegradation of methylene blue (MB) under visible-light irradiation ($\lambda \geq 420$ nm) as a probe reaction, and the preliminary results are shown in Figure 5. Prior to the photodegradation tests, all samples were annealed in air to remove the amorphous carbon, which was formed on the surface of the TiO_2 nanocrystals and served as a barrier against the ripening of TiO_2 nanocrystals during the decomposition of the Ti-hybrid film in H_2/Ar. The annealing temperature has an important effect on the photocatalytic behavior of N-doped TiO_2/CNCs. As shown in Figure 5a, the photocatalytic activity was obviously enhanced after calcination of the N-doped TiO_2/CNCs, coated with 200 MLD cycles, in air from 300 to 400 °C. The sample calcined at 350 °C exhibited the best performance. On the one hand, the surface area of the N-doped TiO_2/CNCs increases after removal of the amorphous carbon (Table S1), resulting in more adsorbed MB and a faster decomposition rate for MB. On the other hand, a higher temperature (400 °C) leads to aggregation of TiO_2 and decreases its photocatalytic activity because of a lower surface area (Figure S5 and Table S1). XPS analyses show that the peak positions of N 1s of the samples before (Figure 3b) and after (Figure S6) annealing in air at 350 °C are identical and that their N/Ti atomic ratios are 0.26 and 0.27, respectively, indicating that the nature of nitrogen and its content keep nearly unchanged after annealing in air.

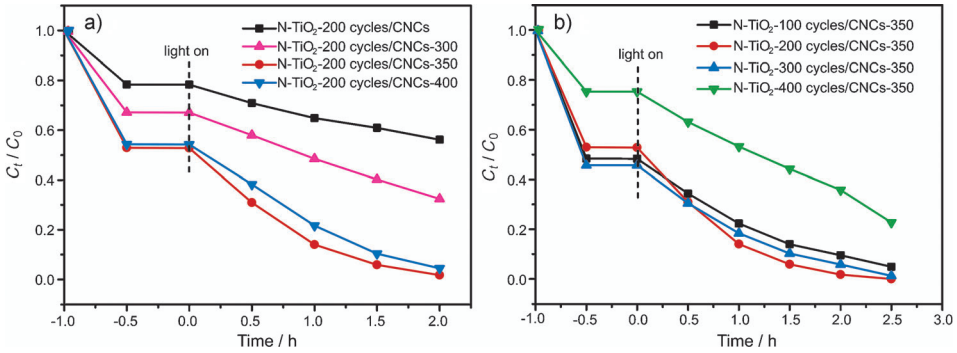

Figure 5. Photocatalytic degradation of MB under visible light irradiation monitored as the normalized concentration change versus irradiation time for different samples (C_t is the concentration of MB at the irradiation time t and C_0 is the initial concentration). a) For nanoporous N-doped TiO_2/CNCs (produced with 200 MLD cycles) after removal of amorphous carbon by annealing in air at different temperatures. b) For nanoporous N-doped TiO_2/CNCs produced with varying MLD cycles after removal of amorphous carbon by annealing in air at 350 °C.

Figure 5b shows the photocatalytic performance of N-doped TiO_2/CNCs with varying MLD cycle numbers and under fixed annealing conditions (350 °C in air). With an increasing MLD cycle number from 100 to 400, the activity of N-doped TiO_2/CNCs initially increased and subsequently decreased. The N-doped TiO_2/CNCs with 200 MLD cycles showed the fastest decomposition rate for MB, probably because of the best matching of TiO_2 content and shorter diffusion length, which stands in correlation to the MLD film thickness. The nanoporous structure and the nanoscale thickness of the N-doped TiO_2 film prepared by MLD favor the MB molecules to quickly adsorb to the N-doped TiO_2 nanocrystals, which then act as catalytic sites to degrade the molecules under visible light irradiation, making the N-doped TiO_2/CNCs exhibit excellent photodegradation activity in visible light. The photocatalytic activity of porous N-doped TiO_2/CNCs under visible light irradiation is in strong contrast to the very low activity of un-doped TiO_2/CNCs prepared by coating carbon nanocoils with $TiCl_4$ and H_2O as precursors (Figure S7). For comparison, the photocatalytic activity of N-doped TiO_2/CNCs under ultraviolet light ($\lambda = 365$ nm) irradiation was also investigated, revealing a much higher activity than under visible light irradiation (Figure S8).

In conclusion, a novel MLD method based on a four step ABCB reaction sequence using $TiCl_4$, ethanolamine, and malonyl chloride as the reactants has been demonstrated for depositing Ti-hybrid films on surfaces of CuO nanowires and CNCs. The reaction includes a hetero-bifunctional organic precursor and a homo-bifunctional organic precursor, both ensuring a certain selectivity of the coupling reactions in each step of the process and allowing a combinatorial approach to organic–inorganic hybrid materials through control of the functional groups of the molecules. The four coupling sites used herein (metal halide, acyl chloride, amine, and alcohol) offer a wide variety of tuning possibilities for the composition of the organic–inorganic hybrid film and the resulting chemical and physical properties. An adaptation of the methodology implies a variety of possibilities for tuning the distance between adjacent Ti ions and thus the Ti content in the hybrid film by selecting the chain length of the organic linkers and even modification of processes towards ABCBCBA or further pulsing sequences. Under annealing in H_2/Ar, the obtained Ti-hybrid materials transformed into nanoporous N-doped TiO_2 nanotubes and nanoporous N-doped TiO_2/CNCs, respectively. The TG-MS results showed that nitrogen doping occurred through a reaction of TiO_2 with NH_3, which was generated in situ by decomposition of the amide-containing organic components. The nanoporous N-doped TiO_2/CNCs obtained after applying 200 MLD cycles exhibited excellent photocatalytic activity for the degradation of MB even with visible light. This synthesis method can be further extended to fabricate other hybrid and after annealing nanoporous materials as shown on the example of Al_2O_3.

Experimental Section

MLD process: The CNCs used in this work were synthesized by chemical vapor deposition using acetylene as a carbon source and copper nanoparticles as catalysts at 250 °C, followed by a heat

treatment at 900 °C in Ar atmosphere for 1 h as reported previously.[36] The MLD process was carried out in a hot-wall closed chamber-type ALD reactor. Prior to MLD, the CNCs were dispersed in ethanol by ultrasonic agitation and then dropped onto a quartz wafer. After being air-dried, the Ti-hybrid films were deposited by sequential exposure of the CNCs to $TiCl_4$, ethanolamine, malonyl chloride, and ethanolamine. The deposition temperature was 100 °C. The temperature of the ethanolamine source was kept at 80 °C. After the MLD process, the samples were transferred to a furnace and annealed at 600 °C in 5 % H_2/Ar atmosphere for 2 h.

Characterization: XRD patterns were collected on a Bruker D8 Advanced X-ray Diffractometer. TEM and HRTEM images were taken with a JEOL-2100F microscope. The samples for TEM analysis were prepared by dropping an ethanol droplet of the products on carbon-coated copper grids and drying at room temperature. FTIR spectra were recorded with a Bruker Tensor 27 instrument. For the XPS analysis, a Kratos AXIS 165 multitechnique electron spectrometer was used. The surface area of the products was measured by the Brunauer–Emmet–Teller (BET) method using N_2 adsorption and desorption isotherms on an Autosorb-1 analyzer. TG-MS studies were performed using a thermogravimetric analyzer (SETARAM, Evolution 16/18) coupled with an on-line mass spectrometer (Balzers, Ominstar; heating rate 10 °C min^{-1}, argon flow). The voltage of the electron source was 40 eV, and the used detector was a multi-channel type with a voltage of 950 V. The variation of the contents of H_2O, CO_2, CH_4, and NH_3 was detected at the same time.

Photocatalytic activity tests: The photocatalytic experiments were performed based on the degradation of the methylene blue (MB) solution under visible-light irradiation. In a typical measurement, 10 mg of the sample was added into 30 mL of organic pollutant solution (2.5×10^{-5} M) followed by stirring. After continuous stirring in the dark for 1 h to ensure an adsorption/desorption equilibrium of MB, the suspension was irradiated by a xenon lamp with an optical filter cutting off wavelengths below 420 nm. At regular time intervals, 2 mL portions of the suspension were removed and centrifuged at 12000 rpm (rotations per minute) for 10 minutes to remove the catalysts before UV/Vis measurements were performed for monitoring the concentration change of MB.

Received: March 19, 2013
Revised: June 23, 2013
Published online: July 10, 2013

Keywords: metal oxides · molecular layer deposition · organic–inorganic hybrid composites · photocatalysis · photochemistry

[1] A. Kim, M. A. Filler, S. Kim, S. F. Bent, *J. Am. Chem. Soc.* **2005**, *127*, 6123 – 6132.
[2] B. H. Lee, M. K. Ryu, S.-Y. Choi, K.-H. Lee, S. Im, M. M. Sung, *J. Am. Chem. Soc.* **2007**, *129*, 16034 – 16041.
[3] H. Zhou, S. F. Bent, *ACS Appl. Mater. Interfaces* **2011**, *3*, 505 – 511.
[4] Y. Du, S. M. George, *J. Phys. Chem. C* **2007**, *111*, 8509 – 8517.
[5] N. M. Adamczyk, A. A. Dameron, S. M. George, *Langmuir* **2008**, *24*, 2081 – 2089.
[6] Y.-h. Li, D. Wang, J. M. Buriak, *Langmuir* **2010**, *26*, 1232 – 1238.
[7] S. M. George, B. Yoon, A. A. Dameron, *Acc. Chem. Res.* **2009**, *42*, 498 – 508.
[8] A. A. Dameron, D. Seghete, B. B. Burton, S. D. Davidson, A. S. Cavanagh, J. A. Bertrand, S. M. George, *Chem. Mater.* **2008**, *20*, 3315 – 3326.
[9] X. Liang, M. Yu, J. Li, Y.-B. Jiang, A. W. Weimer, *Chem. Commun.* **2009**, 7140 – 7142.
[10] B. Yoon, D. Seghete, A. S. Cavanagh, S. M. George, *Chem. Mater.* **2009**, *21*, 5365 – 5374.
[11] Y. Lee, B. Yoon, A. S. Cavanagh, S. M. George, *Langmuir* **2011**, *27*, 15155 – 15164.
[12] Q. Peng, B. Gong, R. M. VanGundy, G. N. Parsons, *Chem. Mater.* **2009**, *21*, 820 – 830.
[13] A. I. Abdulagatov, R. A. Hall, J. L. Sutherland, B. H. Lee, A. S. Cavanagh, S. M. George, *Chem. Mater.* **2012**, *24*, 2854 – 2863.
[14] S. Ishchuk, D. H. Taffa, O. Hazut, N. Kaynan, R. Yerushalmi, *ACS Nano* **2012**, *6*, 7263 – 7269.
[15] K. Park, Q. Zhang, B. B. Garcia, X. Zhou, Y.-H. Jeong, G. Cao, *Adv. Mater.* **2010**, *22*, 2329 – 2332.
[16] H. Shin, D. K. Jeong, J. Lee, M. M. Sung, J. Kim, *Adv. Mater.* **2004**, *16*, 1197 – 1200.
[17] Y. J. Hwang, C. Hahn, B. Liu, P. Yang, *ACS Nano* **2012**, *6*, 5060 – 5069.
[18] T. Blanquart, J. Niinistö, M. Gavagnin, V. Longo, V. R. Pallem, C. Dussarrat, M. Ritala, M. Leskelä, *Chem. Mater.* **2012**, *24*, 3420 – 3424.
[19] H.-E. Cheng, W.-J. Lee, C.-M. Hsu, M.-H. Hon, C.-L. Huang, *Electrochem. Solid-State Lett.* **2008**, *11*, D81 – D84.
[20] V. Pore, M. Heikkilä, M. Ritala, M. Leskelä, S. Areva, *J. Photochem. Photobiol. A* **2006**, *177*, 68 – 75.
[21] Y. Qin, C. Chen, M. Knez, *12th International conference on atomic layder deposition*, Dresden, Germany, **2012**, 112.
[22] Y. Qin, S.-M. Lee, A. Pan, U. Gosele, M. Knez, *Nano Lett.* **2008**, *8*, 114 – 118.
[23] H. Qian, S. Li, J. Zheng, S. Zhang, *Langmuir* **2012**, *28*, 17803 – 17810.
[24] Y. Qin, Y. Kim, L. Zhang, S.-M. Lee, R. B. Yang, A. Pan, K. Mathwig, M. Alexe, U. Gösele, M. Knez, *Small* **2010**, *6*, 910 – 914.
[25] G. Wang, Z. Gao, S. Tang, C. Chen, F. Duan, S. Zhao, S. Lin, Y. Feng, L. Zhou, Y. Qin, *ACS Nano* **2012**, *6*, 11009 – 11017.
[26] C. Marichy, J.-P. Tessonnier, M. C. Ferro, K.-H. Lee, R. Schlogl, N. Pinna, M.-G. Willinger, *J. Mater. Chem.* **2012**, *22*, 7323 – 7330.
[27] E. R. Cleveland, P. Banerjee, I. Perez, S. B. Lee, G. W. Rubloff, *ACS Nano* **2010**, *4*, 4637 – 4644.
[28] L. J. Gerenser, J. M. Grace, G. Apai, P. M. Thompson, *Surf. Interface Anal.* **2000**, *29*, 12 – 22.
[29] T. Strother, R. J. Hamers, L. M. Smith, *Nucleic Acids Res.* **2000**, *28*, 3535 – 3541.
[30] J. Fang, F. Wang, K. Qian, H. Bao, Z. Jiang, W. Huang, *J. Phys. Chem. C* **2008**, *112*, 18150 – 18156.
[31] O. Diwald, T. L. Thompson, T. Zubkov, S. D. Walck, J. T. Yates, *J. Phys. Chem. B* **2004**, *108*, 6004 – 6008.
[32] X. Wang, T.-T. Lim, *Appl. Catal. A* **2011**, *399*, 233 – 241.
[33] G. Liu, L. Wang, C. Sun, Z. Chen, X. Yan, L. Cheng, H.-M. Cheng, G. Q. Lu, *Chem. Commun.* **2009**, 1383 – 1385.
[34] H. Irie, Y. Watanabe, K. Hashimoto, *J. Phys. Chem. B* **2003**, *107*, 5483 – 5486.
[35] S. Hoang, S. P. Berglund, N. T. Hahn, A. J. Bard, C. B. Mullins, *J. Am. Chem. Soc.* **2012**, *134*, 3659 – 3662.
[36] Y. Qin, Z. Zhang, Z. Cui, *Carbon* **2004**, *42*, 1917 – 1922.

